This reporting period between Jan. – Sept. 2023 represents the last stage of the project implementation. As a general conclusion we can affirm that the proposed activities have been performed, and the specific objectives have been acieved, however during the project implementation we encountered several problems which were not foreseen from the project proposal perspective. We considered these unforeseen problems as challenges to be addressed.

In order to optimize the workflow process we have **moved our data generation computer code** from Fortran to Python. This implied that we had to newly develop the generation code for FROG traces and the spectral fields associated with them (labels). We have generated with this version a new dataset, which displays a richer variety in terms of the spectral amplitude and phase. The spectral amplitude is now defined as a sum of Gaussian functions. The number of Gaussians is generated randomly between 10 and 30. We also generate randomly the spectral widths of the Gaussian functions in the [10, 30] nm interval, as well as the central wavelength of these functions which are generated around the reference value of 800 nm in the interval [793, 807] nm. Employing these spectral amplitudes and adding the random phase term, the spectral field of the pulse is obtained. The spectral field is inverse Fourier transformed to obtain the pulse in the time domain, *E(t)*, which along with its time delayed replica is used to generate a FROG spectrogram (image). We also increased the number of samples generated to around *300000* to ensure a more diverse representation of the simulated laser pulses. However, generating larger datasets puts a demand on our storing capabilities of the different datasets, since only this lastly generated dataset (with all associated files) needs around 70 Gb of space. We split the dataset into three subsets representing 80%, 10% and 10% of the total samples: training set, validation set and test set, respectively.

The neural network was trained with the training set, with a Gaussian noise (mean = 0, std = 0.15) added to the FROG traces during training. The validation set was employed to detect potential overfitting behavior of the network, while the test set is used to evaluate the performance of the convolutional neural network. We emphasize here that our current test set is about *30000* samples and these are data never used during training. This new test set is about three times

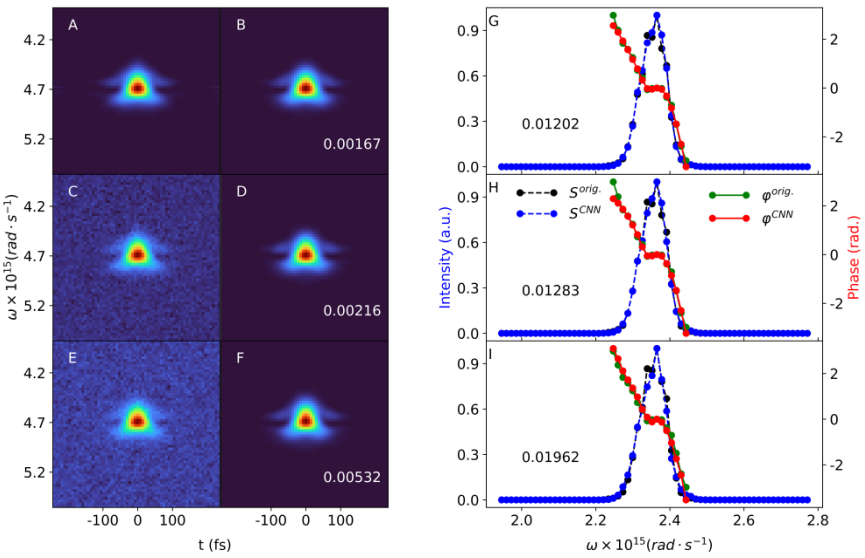

Fig. 1 Reconstruction of a computer simulated pulse. (Panels A, C, E): original FROG traces with different noise levels. (Panels B, D, F): reconstructed FROG traces showing the FROG reconstruction error. (Panels G, H, I): black dashed line with circles: original intensity; blue dashed line with circles: CNN retrieved intensity; green line with circles: original spectral phase; Red line with circles: CNN reconstructed spectral phase. Panels G, H, I also show the l_1 reconstruction error for the pulses as detailed in the text.

larger than our previous one.

In Fig. 1 we show one example of our **simulated FROG images** and pulses. The reconstruction is performed for FROG traces, which enter the CNN with different noise levels. The first column contains the original FROG trace with increasing noise level from top to bottom. A: zero noise; C: Gaussian noise with *mean = 0* and *std = 0.15*; E: Gaussian noise with *mean = 0* and *std = 0.2*. In the third column we plotted the reconstructed spectral intensities and phases corresponding to the three FROG images. Panels G, H and I show these quantities as a function of the angular frequency. In all three cases, a good agreement between the original and the reconstructed spectral quantities is observed. This is confirmed also by the reconstruction error (l_1 loss) calculated in every case. For a single FROG trace the reconstruction time is on the millisecond scale (*~30 ms*) on a 2.2 GHz computer. We also calculated the mean l_1 loss for the entire test set, which are 0.022199, 0.022286 and 0.024890, respectively for increasing noise levels. The reconstructed spectral intensity and phase are used to reconstruct the FROG trace itself for all the noise levels mentioned above. The reconstructed FROG traces are plotted in the second column of Fig. 1 (panels B, D and F), along with the FROG reconstruction error. It may be observed a very good similarity between the original and reconstructed FROG images. The reconstruction of the pulses and the FROG

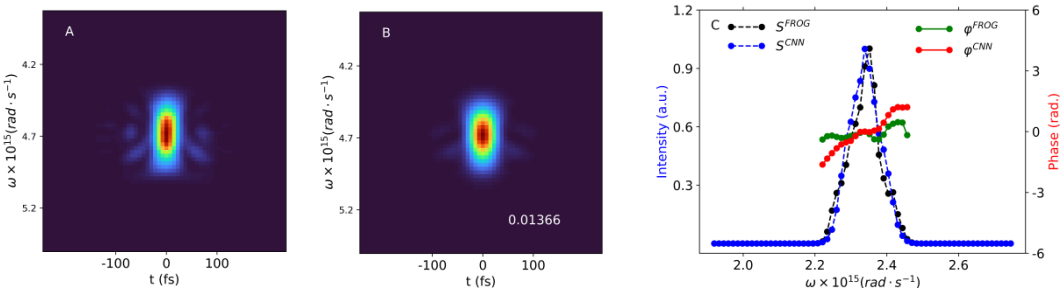

Fig 2. Reconstruction of an experimental ultrashort laser pulse. (Panel A): experimental FROG trace. (Panel B): retrieved FROG trace showing the FROG reconstruction error. (Panel C): black dashed line with circles: intensity retrieved by GRENOUILLE's built-in algorithm; blue dashed line with circles: CNN retrieved intensity; green line with circles: spectral phase retrieved by GRENOUILLE's built-in algorithm; red line with circles: CNN reconstructed spectral phase.

is also performed in Python now.

We tested our trained CNN on an **experimentally measured SHG-FROG trace**, shown in Fig. 2 (panel A). The experimental FROG trace of laser a pulse centered at 800 nm was measured with GRENOUILLE (a variant of FROG) by our collaborators at the Center for Relativistic Laser Science, Institute for Basic Science (IBS CoReLS), Gwangju, Korea. The grid size of the measured FROG traces was 64 with a delay increment of 7.5 fs. In panel C of Fig. 2 we plotted the retrieved spectral intensity and phase, where we compared the results of two different reconstruction algorithms: the GRENOUILLE's built-in algorithm and our CNN method. The general trend of the curves agrees for both retrieval methods. More specifically the spectral phases overlap along a certain frequency range, where the intensity has significant values. The spectral intensities show similar shapes for both retrieval algorithms. However, there are also obvious discrepancies between the curves retrieved by GRENOUILLE's built-in

algorithm and our CNN. According to the GRENOUILLE's software, the FWHM duration of the first pulse is 28.7 fs, while our method gives 30 fs FWHM duration. Panel B on Fig. 2 shows our retrieved FROG spectrogarm. Again, one may observe good similarities between the retrieved and the experimental FROG traces, for example our method reproduces nicely some of the 'wings' observed in the experimental FROG. The FROG reconstruction error between the experimental and our CNN retrieved FROG trace is 0.01366. The same error in case of GRENOUILLE's built-in software is 0.00844 Given that the CNN was trained with computer generated FROG traces, this is a remarkable performance, and in the same time a very fast pulse reconstruction process.

Regarding the problem of wavefront sensing and controlling its distortions we addressed basic problems, perfomed experiments and made significant progress.
Most characterization devices **assume** flat wavefront of the pulse at the entrance, although (un)intended wavefront distortions characterize the pulses. Controlled wavefront distortions can be introduced using the deformable miorror on all six arms of the HPLS laser system at ELI-NP. It was possible to use the 100 TW output of the HPLS laser system to study such distortions of the wavefront during the experimental campaign awarded at the end of 2022.
One direction of the investigation during the campaign was to **introduce controlled wavefront distortion**, helical phase in shape. It is known that such wavefront shapes generate a doughnut type focal spot which is beneficial in proton acceleration experiments [1]. The doughnut shape is sensitive to the wavefront quality, but also to the presence of spatio-temporal distortions of the pulses [2,3]. In this way, the far field of the helical pulses generated using 1 J pulses in HPLS provides a clear signature of minute wavefront distortions existing in the laser chain.
The experimental study of the **residual wavefront optimization** using helical phaseplate and deformable mirror took place at the ELI-NP facility, more precisely on the 100 TW arm as depicted in Fig. 3. A diagnostic bank is installed there directly after the compressor in the main laser hall, before the beam transport to the 100 TW experimental area E4. Among other things, the diagnostic bank features a Shack-Hartmann WFS (M PLQ HASO4 FIRST 0919 by Imagine Optic) and FF camera (acA1300-60gm by Basler, delivering 8-bit images), which aid the control of the DM (ILAO Star by Imagine Optic, 30 mm pupil, 25 actuators) and inspect the beam focus quality, respectively. At this location, the beam line features a nominal beam diameter of 55 mm, a repetition rate of 10 Hz and a pulse energy of up to 2.3 J within 24 fs at a central wavelength of 808 nm and a bandwidth of 57 nm.

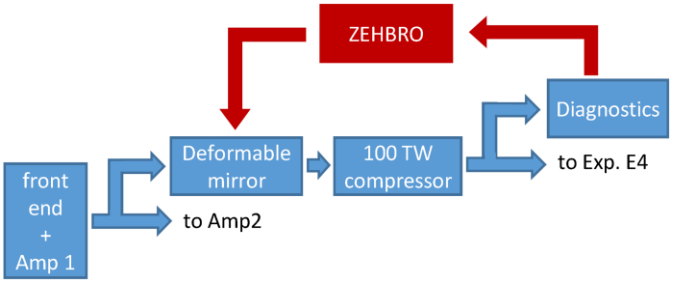

Fig. 3. Control loop for wavefront control in the experiment at the HPLS 100TW output. ZEHBRO stands for the Zernike-coefficient Extraction via Helical Beam Reconstruction for Optimization in the far field [4]

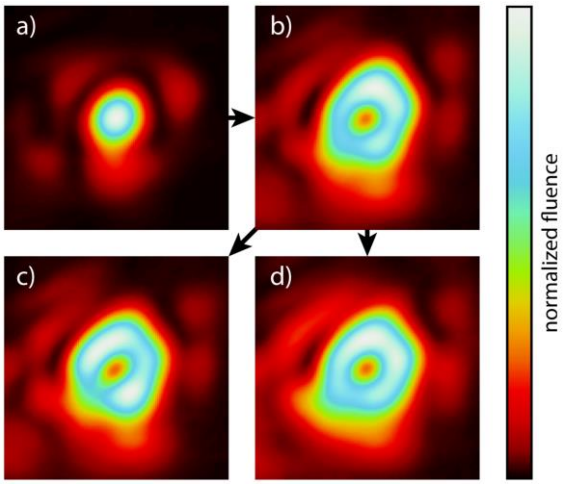

Fig. 4. FF distributions at the compressor sensor. The images where created by centering and averaging 300 images, equal to 30 seconds of operation. a) The FF prior to the insertion of the spiral phase plate, b) after insertion of the phase plate, c) after conventional manual optimization and d) after optimization using ZEHBRO. [4]

A transmitting helical phase plate with 16 discrete levels is inserted in the beam in order to obtain the "donut" beam, using a motorized translation stage. The phase plate is manufactured from fused silica and optimized for the central wavelength of the beam. Due to the wavelength dependence of the material, the outer parts of the spectrum experience a non-perfect helix. For obvious reasons, the phase plate must be installed before the compressor to avoid nonlinear effects with the temporally compressed pulse. In addition, the maximum allowed energy was reduced to 1 J to keep intensity modulations, caused by the phase discontinuity of the phase plate, below the damage threshold of the compressor gratings and components in the following laser beamline.

The deformable mirror was adjusted with different perturbations, of the order of 0.05 λ, for different low order Zernicke modes. Following the algorithm developed at GSI, the far field is used to extract the corrections for the wavefront, as illustrated in Fig. 4d.

We also transported the pulses to the experimental area E4, few tens of meters from the compressor. There we were able to re-optimize the doughnut spot recorded with a spectral filter and we also identified the signature of the presence of spatial chirp in the pulse, as predicted in [3].

[1] C. Brabetz, S. Busold, T. Cowan, O. Deppert, D. Jahn, O. Kester, M. Roth, D. Schumacher, V. Bagnoud 2015; Laser-driven ion acceleration with hollow laser beams. Phys. Plasmas; 22 (1): 013105. https://doi.org/10.1063/1.4905638

[2] Talposi, A.-M., Ursescu, D., 2022. Propagation of ultrashort laser fields with spatiotemporal couplings using Gabor's Gaussian complex decomposition. Journal of the Optical Society of America A 39, 267–278. https://doi.org/10.1364/josaa.444989

[3] Talposi, A.-M., Iancu, V., Ursescu, D., 2022. Influence of Spatio-Temporal Couplings on Focused Optical Vortices. Photonics 9, 389. https://doi.org/10.3390/photonics9060389

[4] Ohland, J.B., Posor, D., Eisenbarth, U., Iancu, V., Ungureanu, R., Ursescu, D., Bagnoud, V., Zernike-coefficient Extraction via Helical Beam Reconstruction for Optimization (ZEHBRO) in the far field, High Power Laser Science and Engineering 1–11 (2023), accepted. https://doi.org/10.1017/hpl.2023.63